Third-order frequency-resolved photon correlations in resonance fluorescence

Yamil Nieves and Andreas Muller

Phys. Rev. B **98**, 165432 — Published 22 October 2018

DOI: 10.1103/PhysRevB.98.165432

Third-Order Frequency-Resolved Photon Correlations in Resonance Fluorescence

Yamil Nieves and Andreas Muller*
Physics Department, University of South Florida, Tampa, Florida
(Dated: September 17, 2018)

We investigated third-order correlations between photons born in single quantum dot resonance fluorescence that were filtered with narrow-band tunable etalons. Three-time autocorrelation measurements in which photons were identically filtered resulted in correlation maps that are functions of two relative delays. A comparison with the correlation maps computed using the "sensors method" introduced by del Valle *et al.* [Phys. Rev. Lett. **109**, 183601 (2012)] reveals faithful agreement with theory, with the strongest correlations obtained when filtering between Mollow triplet sidebands and the central peak. We characterized the correlations associated with these virtual transitions, and compared them with correlations at other Mollow triplet frequency windows. Accentuated nonclassical characteristics are amongst the distinguishing features of three photon spectra.

PACS numbers: 78.67.Hc, 78.47.–p, 78.55.Cr

I. INTRODUCTION

Photon correlations are the primary tool for characterizing light-matter interactions at the few or single quantum level. In principle, if photon correlation functions to all orders were known, all measurable properties of a given light source would be known.

The first-order photon correlation function, $g^{(1)}(\tau_1)$, of a light source is readily obtained interferometrically; its Fourier transform is the power spectrum. Although it provides invaluable information about the light and the mechanism underlying its generation, a $g^{(1)}(\tau_1)$ measurement alone reveals little about the source itself. For example, a light source consisting of a single radiating atom, and a light source consisting of an ensemble of non-interacting radiating atoms could have identical $g^{(1)}(\tau_1)$. To distinguish the two, a second-order photon correlation measurement is required; the single atom source would uniquely exhibit photon anti-bunching [1]. The second-order correlation function, $g^{(2)}(\tau_1, \tau_2)$, is proportional to the histogram of photon arrival time differences between two detection channels and has been used extensively in the past decades to characterize a variety of light sources such as lasers and single photon emitters [2–7]. Crucially, a $g^{(2)}(\tau_1, \tau_2)$ measurement serves as a unique identifier of non-classical light sources, i.e., sources of light which cannot be described without quantum theory [8].

Recently, there has been increasing interest in correlation measurements which go beyond second order. Early work using a streak camera showed strong photon bunching statistics in third-order correlation measurements of microcavity laser light [9, 10]. The third-order correlation function, $g^{(3)}(\tau_1, \tau_2, \tau_3)$, was shown to provide more refined information about nonclassical light sources such as multiphoton differentiation [11] and the ability to analyze components [12]. Most recently, the nonclassical character of light emitted by a strongly coupled quantum dot-cavity system has been demonstrated up to fourth order [13]. For a wide range of quantum processes, including those involving multiparticle interactions [14], photon correlations are an enabling investigative tool which is now more powerful than ever thanks to increasingly performant detection systems [15].

A fascinating development in the understanding of photon statistics has been the generalization of *frequency-resolved* photon correlations. The pioneering theoretical work of del Valle *et al.* has introduced a method for computing the "N-photon spectrum" $g^{(N)}_{\Gamma_1 \ldots \Gamma_N}(\tau_1, \omega_1; \ldots; \tau_N, \omega_N)$, which is proportional to the joint probability of detecting a photon in channel 1 at time τ_1 filtered at frequency ω_1 with a bandwidth Γ_1, a photon in channel 2 at time τ_2 filtered at frequency ω_2 with a bandwidth Γ_2, ..., and a photon in channel N at time τ_N filtered at frequency ω_N with a bandwidth Γ_N [16]. An interesting aspect of $g^{(N)}_{\Gamma_1 \ldots \Gamma_N}(\tau_1, \omega_1; \ldots; \tau_N, \omega_N)$ is that it reveals information about pathways underlying the generation of light in a given source [5]. Although the computation of such a function is challenging using direct integration, the "sensors method" of Ref. 16 makes the calculation straightforward even at high orders. Recently, we have experimentally measured the function $g^{(2)}_{\Gamma_1 \Gamma_2}(\tau_1, \omega_1; \tau_2, \omega_2)$, a two-photon spectrum, and verified distinguishing features predicted by theory such as the existence of "leap-frog" transitions [4].

Here we explore third order correlation functions which make up the three-photon spectrum $g^{(3)}_{\Gamma_1 \Gamma_2 \Gamma_3}(\tau_1, \omega_1; \tau_2, \omega_2; \tau_3, \omega_3)$ of single quantum dot (QD) resonance fluorescence under strong monochromatic laser illumination. Contrary to its second-order counterpart, the function $g^{(3)}_{\Gamma_1 \Gamma_2 \Gamma_3}(\tau_1, \omega_1; \tau_2, \omega_2; \tau_3, \omega_3)$ involves three-photon pathways down the ladder of dressed states, adding a new dimension to potential communication schemes in quantum information science applications [17]. Our measurements provide further confirmation of the validity of the method of Ref. 16 and may lead to more advanced experiments, such as those involving heralded photon bundles [18].

* mullera@usf.edu

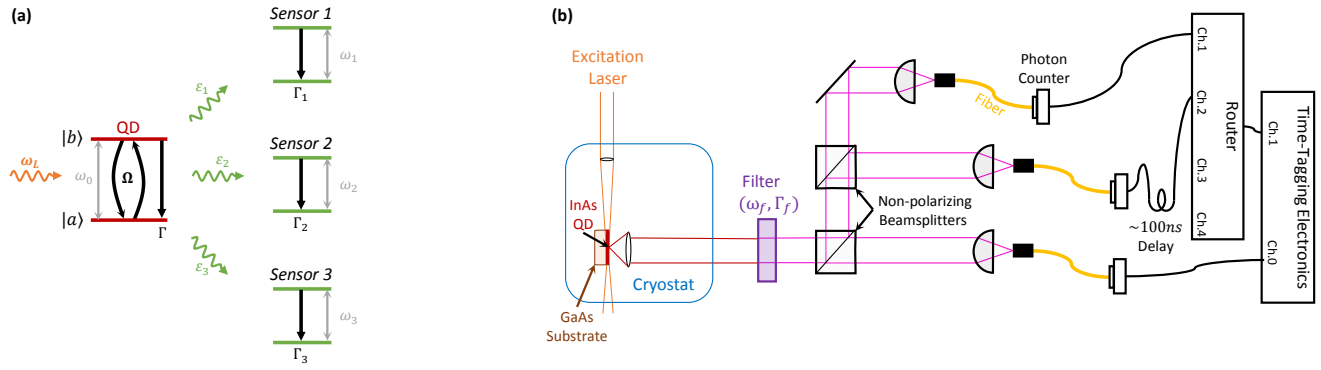

FIG. 1. (a) A resonantly-driven two-level system generating resonance fluorescence is weakly coupled to three sensors so that correlations between sensor populations are proportional to filtered resonance fluorescence intensity correlations. (b) Experimental setup: the light near-resonantly scattered by a strongly-driven QD excitonic two-level system was collected by a lens, spectrally filtered, split three ways and detected. Time-tagging was performed on each channel independently.

II. BACKGROUND

Resonance fluorescence is generated when a two-level electronic system is interacting resonantly or very near resonantly with a monochromatic laser. It is well known that under a sufficiently intense applied field, the resonance fluorescence spectrum consists of a "Mollow triplet" centered at the laser frequency, with individual peaks approximately separated by the Rabi frequency, Ω [19]. The light emission process may be viewed as a cascade down a ladder of dressed-states, i.e., the eigenstates of the coupled light-matter Hamiltonian [1]. Extensively documented for isolated atoms [20], molecules [21], quantum dots [22–26] and Josephson-junctions [27], a two-level system in the Mollow triplet regime serves as a unique platform for testing novel quantum optics concepts. Despite its apparent simplicity, it continues to be researched for its fascinating properties which may benefit emerging quantum information science applications [28].

A N-photon spectrum as a generalization to the ordinary spectrum is one such concept. It is built on the notion of a time-dependent physical spectrum introduced by Eberly *et al.* [29], and of time-dependent correlation functions studied extensively by Knöll *et al.* [30]. At N-th order, however, the computation of such a quantity becomes challenging once $N > 2$ [31]. Del Valle *et al.* proposed and demonstrated that correlations of spectrally filtered photons emitted by a system under test can be calculated by weakly coupling the system to N sensors with a finite bandwidth, Γ_i, and computing correlations between sensor populations, as depicted schematically in Fig. 1(a).

The objective of this work is to test the theory of del Valle *et al.* against experimental measurements for the case of third order correlations. After briefly describing our experimental setup in Section III, we report the measurement of raw two-time correlation maps in Section IV. In Section V, theoretical simulations are presented for comparison. We then present a summary of extracted N-Photon spectra in Section VI and finally provide a simple dressed-states interpretation in the discussion Section VII.

III. EXPERIMENTAL SETUP

From an experimental point of view, a N-photon spectrum measurement is based on a straightforward extension of a Hanbury-Brown and Twiss type measurement, wherein light from a source is split into N channels each equipped with a spectral filter and detector. We probed molecular-beam-epitaxy-grown InAs QDs held in a cryostat (base temperature of 4 K) and interacting with a resonant wave-guided monochromatic laser beam [32]. Our setup, depicted in Fig. 1(b), is optimized to efficiently collect the light scattered by a single QD while minimizing unwanted background laser scattering [22]. We focus here exclusively on autocorrelation measurements, i.e., measurements involving only one filter, a thick solid etalon, whose resonance frequency, ω_f, is tunable [33]. The bandwidth of the filter was fixed at $\Gamma_f/2\pi = 330$ MHz approximately matching the linewidths of the peaks in the Mollow triplet. After traversing the filter the QD scattered light was split three ways by two non-polarizing beam splitters and detected by single photon detector modules (Excelitas SPCM-AQRH-14). Tagging of photon arrival times was performed for each detection channel independently with the help of a router (PicoQuant PHR 800 router with 100 ns cable delay to avoid the router dead-time window) and time-tagging electronics (PicoQuant PicoHarp 300) at an overall detector-limited resolution of about 400 ps. Note that the router is used here for no purpose other than as a replacement for a more expensive multichannel time-tagging system.

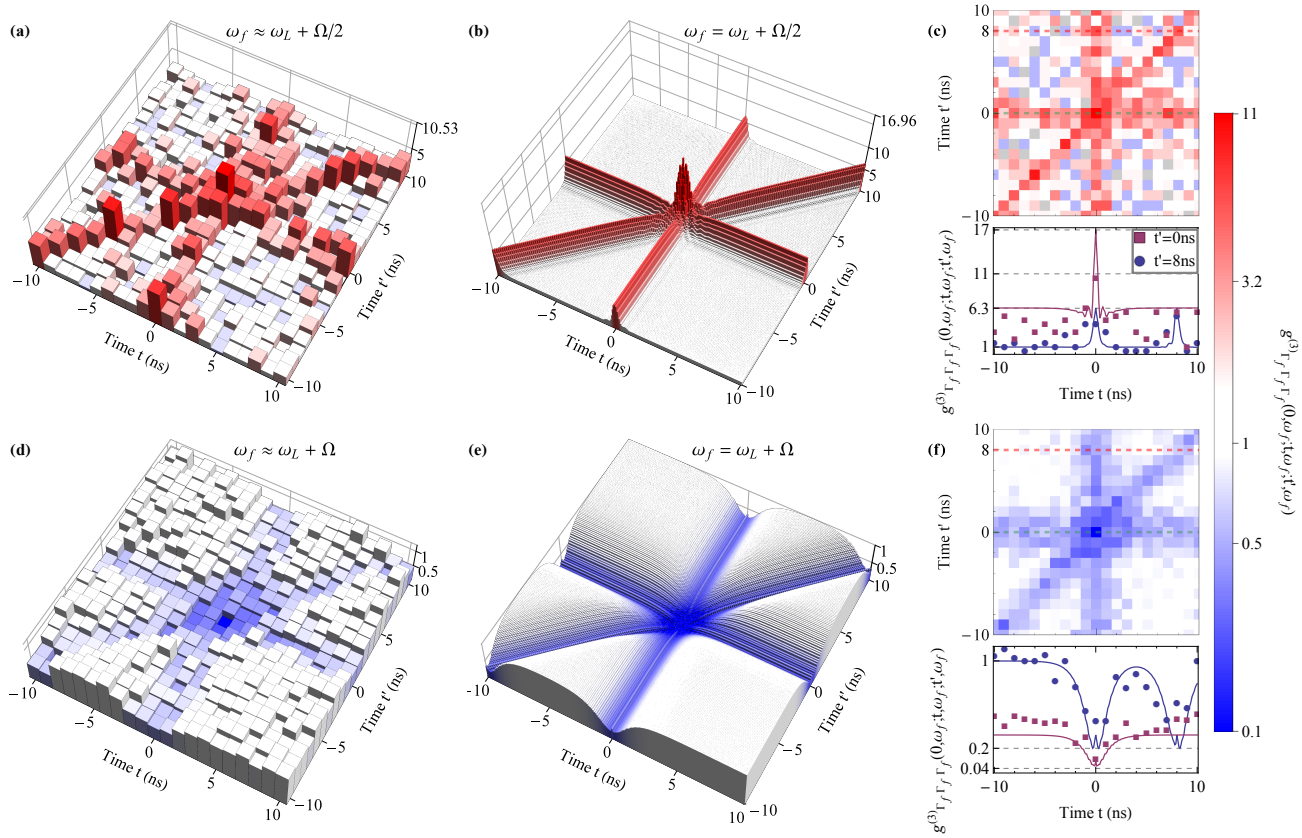

FIG. 2. Experimental (a) and theoretical (b) third-order correlation map for a filtering frequency $\omega_f \approx \omega_L + \Omega/2$ with fixed Rabi frequency $\Omega/2\pi = 1.88\,\mathrm{GHz}$, a radiative decay rate $\Gamma/2\pi = 200\,\mathrm{MHz}$, a filter bandwidth $\Gamma_f/2\pi = 330\,\mathrm{MHz}$ (where $\Gamma_1 = \Gamma_2 = \Gamma_3 = \Gamma_f$), and a laser detunning $\Delta = 0$. (c) (top) corresponding density plot for same data as in part (a) and, (bottom) selected cross-sections as indicated. (d-f) Same as in (a-c) but for a filtering frequency $\omega_f \approx \omega_L + \Omega$.

IV. THREE-PHOTON CORRELATION MAPS

All measurements were performed for a fixed Rabi frequency $\Omega/2\pi = 1.88\,\mathrm{GHz}$. Time tags were stored for each channel separately so that correlation functions could be computed as histograms of arrival time delays between "clicking" detectors. Due to the long exposure times needed to collect sufficiently many third order coincidence events (on the order of hours), we focus here on two specific measurements each with a different filter frequency setting.

In Fig. 2(a), the experimental three photon correlation map with a 1 ns bin width is shown for a filter frequency $\omega_f \approx \omega_L + \Omega/2$. The map reveals a strong coincidence peak at $t = t' = 0$ demonstrating that for this filter configuration photons are more likely to be detected in bunches than spread over time. In addition, the map also reveals diagonal ridges which indicate that events in which two photons are detected simultaneously and one photon is accidental are more frequent than events in which all three detectors "click" accidentally at different times. Selected cross sections at $t = 0$ and $t = 8\,\mathrm{ns}$ through the maps are shown at the bottom of Fig. 2(c) for a more quantitative comparison. In a second configuration, namely for a filter frequency $\omega_f \approx \omega_L + \Omega$, the correlation map looks quite different, as shown in Fig. 2(d-f). For this case, nonclassical correlations are seen at coincidence ($t = t' = 0$) and whenever two out of three detectors click simultaneously, producing anti-bunching troughs.

V. THEORY

To quantitatively describe the frequency-filtered correlation maps of Fig. 2 we turn to a theoretical modeling following the method of del Valle *et al.* For simplicity we describe the QD exciton generating resonance fluorescence as a two-level system radiatively decaying at a rate Γ while being driven by a monochromatic laser at frequency ω_L. The laser may be detuned from the QD resonance frequency, ω_0, by $\Delta = \omega_L - \omega_0$. As detailed in the Appendix, a matrix M [Eq. A1] determines this system's observables such as $\langle a \rangle$, $\langle a^\dagger \rangle$, and $\langle a^\dagger a \rangle$, at time τ, where $a^\dagger$ and a denote the creation and annihilation operators of the resonance fluorescence photons, assumed proportional to the two-level system creation and annihilation operators [19].

In order to describe filtered photon correlations at any order, del Valle *et al.* considered a larger system, which includes a set of sensors weakly coupled to the QD through the QD resonance fluorescence as depicted in Fig. 1(a). The coupling constants ϵ_i are assumed to be small enough such that these sensors do not disturb the QD in any measurable way. The sensors are most simply modeled as two-level systems with resonance frequencies ω_i, decay rates Γ_i, and creation and annihilation operators $\varsigma_i^\dagger$ and ς_i. The observables of this more general system are conveniently captured by a parameterized vector which for three sensors reads:

$$\mathbf{w}_{[\mu_1\nu_1,\mu_2\nu_2,\mu_3\nu_3]} = \begin{pmatrix} \langle \varsigma_1^{\dagger\mu_1}\varsigma_1^{\nu_1}\varsigma_2^{\dagger\mu_2}\varsigma_2^{\nu_2}\varsigma_3^{\dagger\mu_3}\varsigma_3^{\nu_3}\rangle \\ \langle \varsigma_1^{\dagger\mu_1}\varsigma_1^{\nu_1}\varsigma_2^{\dagger\mu_2}\varsigma_2^{\nu_2}\varsigma_3^{\dagger\mu_3}\varsigma_3^{\nu_3} a\rangle \\ \langle \varsigma_1^{\dagger\mu_1}\varsigma_1^{\nu_1}\varsigma_2^{\dagger\mu_2}\varsigma_2^{\nu_2}\varsigma_3^{\dagger\mu_3}\varsigma_3^{\nu_3} a^\dagger\rangle \\ \langle \varsigma_1^{\dagger\mu_1}\varsigma_1^{\nu_1}\varsigma_2^{\dagger\mu_2}\varsigma_2^{\nu_2}\varsigma_3^{\dagger\mu_3}\varsigma_3^{\nu_3} a^\dagger a\rangle \end{pmatrix}, \quad (1)$$

where μ_i and ν_i are zero or one. In their supplemental material to Ref. 16, del Valle *et al.* provided the system's equation of motion to first order in the couplings ϵ_i, derived from a master equation. For three sensors, this equation of motion reads:

$$\begin{aligned} &\partial_t \mathbf{w}_{[\mu_1\nu_1,\mu_2\nu_2,\mu_3\nu_3]} = \\ &\{M + \mathbb{I}[(\mu_1-\nu_1)i\omega_1 - (\mu_1+\nu_1)\frac{\Gamma_1}{2} + (\mu_2-\nu_2)i\omega_2 - (\mu_2+\nu_2)\frac{\Gamma_2}{2} + (\mu_3-\nu_3)i\omega_3 - (\mu_3+\nu_3)\frac{\Gamma_3}{2}]\}\mathbf{w}_{[\mu_1\nu_1,\mu_2\nu_2,\mu_3\nu_3]} \\ &+ \mu_1(i\varepsilon_1 T_+)\mathbf{w}_{[0\nu_1,\mu_2\nu_2,\mu_3\nu_3]} + \nu_1(-i\varepsilon_1 T_-)\mathbf{w}_{[\mu_1 0,\mu_2\nu_2,\mu_3\nu_3]} + \mu_2(i\varepsilon_2 T_+)\mathbf{w}_{[\mu_1\nu_1,0\nu_2,\mu_3\nu_3]} + \nu_2(-i\varepsilon_2 T_-)\mathbf{w}_{[\mu_1\nu_1,\mu_2 0,\mu_3\nu_3]} \\ &+ \mu_3(i\varepsilon_3 T_+)\mathbf{w}_{[\mu_1\nu_1,\mu_2\nu_2,0\nu_3]} + \nu_3(-i\varepsilon_3 T_-)\mathbf{w}_{[\mu_1\nu_1,\mu_2\nu_2,\mu_3 0]} \end{aligned}, \quad (2)$$

where $\mathbb{I}$ is the identity matrix, and the matrices T_+ and T_- are given in the Appendix [Eq. A5].

Using this equation of motion, any relevant correlation function can be obtained by applying the quantum regression theorem. By repeated applications, the three photon spectrum of the QD resonance fluorescence can then be obtained via correlations between sensor populations $n_i = \varsigma_i^\dagger \varsigma_i$ as

$$g^{(3)}_{\Gamma_1\Gamma_2\Gamma_3}(0,\omega_1;t,\omega_2;t',\omega_3) = \frac{\langle n_1(0) n_2(t) n_3(t')\rangle}{\langle n_1(0)\rangle\langle n_2(0)\rangle\langle n_3(0)\rangle}. \quad (3)$$

All the calculations shown in the present work involved numerically integrating Eq. (2) using Mathematica$^{\text{TM}}$ in a recursive manner as detailed in Appendix A.

Figure 2(b) and Fig. 2(e) show the result of simulations with the same parameters as those of the corresponding experiments. As can be seen, these theoretical maps closely resemble the experimental observations even without including more realistic solid-state processes such as spectral diffusion and phonon scattering [24, 26, 32].

VI. *N*-PHOTON SPECTRA

Before further scrutinizing the third-order correlation maps presented above it is helpful to view them as constituents of a three photon spectrum which can then be discussed using the dressed-state formalism. Following the language of del Valle *et al.* we refer to the coincidence value of the normalized N-th order frequency-filtered correlation function simply as the "N-photon spectrum".

The lowest order function, the one-photon spectrum is then simply proportional to the count rate of one of the detectors, as shown in Fig. 3(a), as a function of ω_f. This is the familiar Mollow triplet at a resolution ω_f. The origin of the three peaks is best visualized using the dressed-states picture, wherein the resonance fluorescence process is interpreted as a cascade down the ladder of superposition states which result from the diagonalization of the coupled QD-laser Hamiltonian [1]. In this picture, the one-photon spectrum emerges out of four transitions, two of which are degenerate and at the laser frequency, ω_L, as indicated in Fig. 3(a). These are the only possible transitions between successive rungs.

The spectrally resolved correlation function of next higher order is the two photon spectrum. It has recently been documented theoretically [18] and experimentally [4] for the case of light scattered by a resonantly driven QD. In general it involves two filter frequencies and must therefore be represented as a two-dimensional map. However, when the two photons emitted are detected at the same frequency as in the single filter experiments discussed here, only the full map's diagonal, as plotted in Fig. 3(b), is relevant. The two photon spectrum then represents the probability of simultaneous emission of two photons at the same frequency. Its most obvious features are two dips positioned at the location of the Mollow triplet sidebands, two peaks located halfway between the central peak and a sideband, and a nearly vanishing peak at the location of the Mollow triplet central peak. The dressed states picture has been used to interpret the origin of these peaks. All possible pathways between states

separated by one rung must now be considered [Fig. 3(b)]. If the upper (lower) state from the upper rung connects the upper (lower) state from the lower rung, then the two photons generated are at the central (laser) frequency. These two pathways interfere to give rise to nearly Poisson statistics [34, 35]. If on the other hand the upper (lower) state from the upper rung connects the lower (upper) state from the lower rung then there can be no real intermediate state and the emitted photon's frequencies are at approximately $\omega_L + \Omega/2$ and $\omega_L - \Omega/2$. Since these two-photon cascades can only proceed through virtual intermediate states, strong correlations are expected and observed experimentally [Fig. 3(b)]. These transitions have been coined "leapfrog" transitions [5]. Lastly, the anti-bunched photon statistics (dips) at the location of the sidebands can be viewed as originating in disconnected pathways.

One order up, the three photon spectrum describes the probability of simultaneous frequency-resolved detection of three photons. The relevant dressed-states transitions are those between states separated by two rungs. For the presently considered case of three photons with the same frequency, the distinguishing pathways are the ones from the upper (lower) state of the upper rung to the lower (upper) state of the lower rung which necessarily must proceed via two virtual intermediate states, and require the photons to have frequencies of approximately $\omega_L + \Omega/3$ and $\omega_L - \Omega/3$. This sequential photon emission is in fact observed in our experimental data plotted in Fig. 3(c).

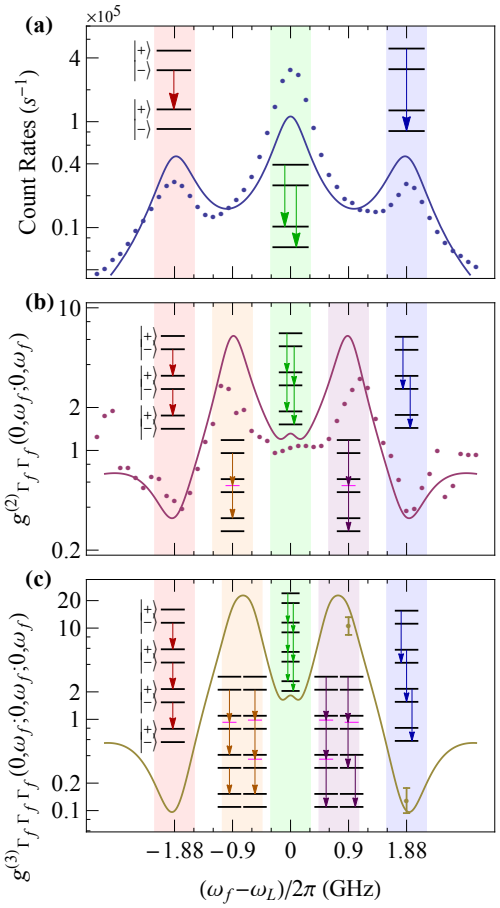

FIG. 3. First (a), second (b) and third (c) order filtered resonance fluorescence intensity correlations as a function of filter resonance frequency ω_f relative to the laser frequency ω_L with same parameters as Fig. 2. Dressed-state diagrams illustrate the transitions each located at their corresponding filter frequency (i.e., $\omega_f = \omega_L \pm (0, \Omega/3, \Omega/2, \Omega)$.

VII. DISCUSSION

In order to better understand the presence of the ridges and troughs in the maps of Fig. 2, we turn to simulated maps where the only difference from those shown in Fig. 2 is an increased Rabi frequency, specifically $\Omega/2\pi = 15\,\mathrm{GHz}$. It then is revealed that what seemed to be single correlation peaks in the three photon spectrum of Fig. 3(c) are actually two pairs of correlation peaks. One set of peaks at $\omega_f \approx \omega_L \pm \Omega/3$ is associated with leap-frog transitions over three rungs of the dressed states ladder whereas the other set of peaks at $\omega_f \approx \omega_L \pm \Omega/2$ is due to transitions in which only two of the three photons are connected by a transition through a virtual intermediate state. Accordingly, the latter are associated with correlation maps exhibiting ridges [Fig. 4(b)] while the former are associated with correlations maps in which the ridges are nearly vanishing relative to the coincidence peak [Fig. 4(c)]. The larger Rabi frequency relative to the filter bandwidth and the QD decay rate is the reason that the peaks can be separably viewed in the three photon spectrum of Fig. 4(a) but not in that of Fig. 3(c). While it is straightforward to increase the Rabi frequency in our experiments by increasing the applied laser's intensity, the emission rate then becomes low enough that the overall recording time becomes impractical. This problem can likely be remedied by improving the collection and propagation efficiency, as well as the detector quantum efficiency in our experiments (combined these amount to ≈1% here). In addition, other more complex approaches have been proposed to overcome the reduced emission rate with increased Rabi frequency, such as the use of photonic nanowires [36], microlenses [37], broadband enhancement solution using bullseye structures [38], and using the Purcell effect of cavity quantum electrodynamics [39] to enhance the rate of emission. Then, according to the simulations of Fig. 4(a), correlations larger by many orders of magnitude than in the current experiments may be obtained. Comparing correlations measured for second and third order it can nevertheless already be seen that a three photon spectrum provides more pronounced photon anti-bunching compared to the two-photon spectrum when the filter frequency matches the Mollow triplet sidebands, in addition to increased correlations when the filter frequency is between a sideband and the central peak.

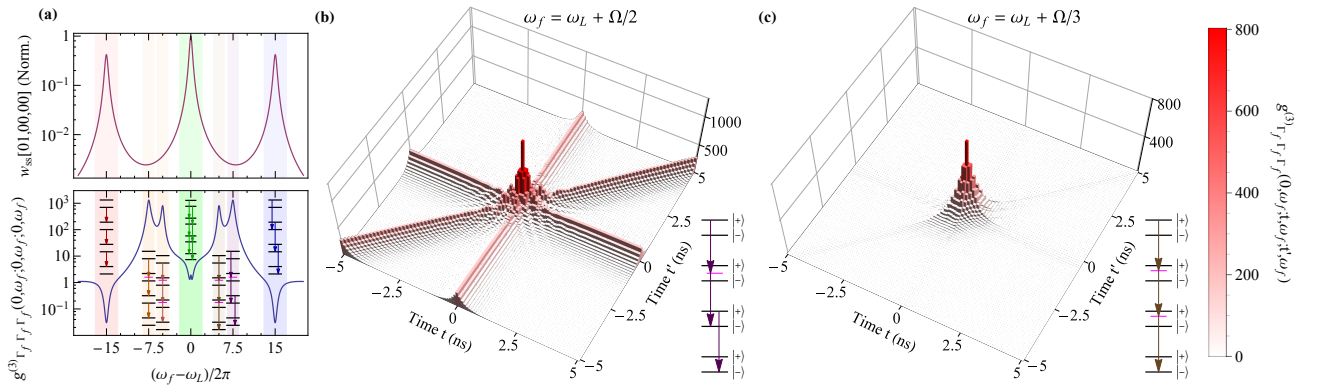

FIG. 4. Simulated third-order correlations for which all parameters are identical to those in Figs. 2 and 3 except for the Rabi frequency, which is now $\Omega/2\pi = 15$ GHz. Part (a) shows the normalized one photon spectrum (top) and the diagonal of the three photon spectrum at zero time delay (bottom), whereas parts (b) and (c) show correlation maps at selected filter frequencies of $\omega_L + \Omega/2$, and $\omega_L + \Omega/3$, respectively.

An interesting prospect emerging from the N-photon spectrum measurement and analysis is the possibility of generating heralded emission of groups of photons of any desirable number. Such photon bundle emission is due to the structure of the dressed-states ladder system. For example, when considering the pathways analyzed in Fig. 4(c)] which consist of three photons emitted subsequently, it is clear that no second such sequence is allowed immediately following the first since the system is left in a lower dressed state. Therefore, there is a tendency to emit in bundles in between other emission events. This feature has been analyzed in detail theoretically and was explicitly verified using Monte Carlo simulations [16]. With the use of independently tunable filters, a large parameter space exists to select pathways for the generation of heralded N-photon sequences [17].

VIII. CONCLUSION

In conclusion, spectrally-filtered third-order photon correlations were recorded for resonance fluorescence from an individual semiconductor QD. Only a single filter was used, thus yielding the autocorrelation cross-section of the complete three-photon spectrum as introduced by del Valle *et al.* Our measurements establish a firmer foothold of this concept and show its utility for characterizing non-classical light sources. The three-photon spectrum exhibits significantly more pronounced photon antibunching compared to its two-photon counterpart. In addition, three photon pathways through virtual states are found to lead to more strongly correlated emission than at second order. Future directions include the measurement of cross-correlations at third-order, i.e. the use of independently tunable filters for each channel which brings about new experimental challenges. Extension to fourth order and heralded photon bundle generation are also possible in principle.

IX. ACKNOWLEDGMENTS

The authors acknowledge financial support from the National Science Foundation (NSF Grant No. 1254324).

Appendix A: Three photon spectrum calculation

The master equation describing the evolution of the density matrix for the QD-laser system leads to an equation of motion for the system's observables, the inputs of which can be captured in the form of a single matrix:

$$M = \begin{pmatrix} 0 & 0 & 0 & 0 \\ -\Omega/2 & -\Gamma/2 - i\Delta & 0 & \Omega \\ -\Omega/2 & 0 & -\Gamma/2 + i\Delta & \Omega \\ 0 & -\Omega/2 & -\Omega/2 & -\Gamma \end{pmatrix}. \quad \text{(A1)}$$

The quantum regression theorem then states that for any operators X and Y of the system, the evolution of the vector $\mathbf{v}_{X,Y}(\tau)$ defined by:

$$\mathbf{v}_{X,Y}(\tau) = \begin{pmatrix} \langle X(0)Y(0)\rangle \\ \langle X(0)a(\tau)Y(0)\rangle \\ \langle X(0)a^\dagger(\tau)Y(0)\rangle \\ \langle X(0)(a^\dagger a)(\tau)Y(0)\rangle \end{pmatrix}, \quad \text{(A2)}$$

is also determined by M. Specifically it must obey the differential equation:

$$\partial_\tau \mathbf{v}_{X,Y}(\tau) = M\mathbf{v}_{X,Y}(\tau)\,, \quad \text{(A3)}$$

so that the steady-state observables are given by:

$$\mathbf{v}^{\rm ss} = \lim_{\tau\to\infty} \mathbf{v}_{1,1}(\tau) = \lim_{\tau\to\infty} e^{M\tau} \begin{pmatrix} 1 \\ 0 \\ 0 \\ 0 \end{pmatrix}. \quad \text{(A4)}$$

For the larger system which includes the sensors, the relevant equation of motion is Eq. (2) in the main text, wherein two matrices $T_\pm$ are defined which introduce an extra $a^\dagger$ for T_+ and an extra a for T_- between X and Y when acting on $\mathbf{v}_{X,Y}(\tau)$ [16]:

$$T_+ = \begin{pmatrix} 0 & 0 & 1 & 0 \\ 0 & 0 & 0 & 1 \\ 0 & 0 & 0 & 0 \\ 0 & 0 & 0 & 0 \end{pmatrix} \quad \text{and} \quad T_- = \begin{pmatrix} 0 & 1 & 0 & 0 \\ 0 & 0 & 0 & 0 \\ 0 & 0 & 0 & 1 \\ 0 & 0 & 0 & 0 \end{pmatrix}. \tag{A5}$$

These matrices are useful for recursively computing the steady state solutions of Eq. (2) via the algebraic parametrized vector equation:

$$\begin{aligned}\mathbf{w}_{\mathrm{ss}[\mu_1\nu_1,\mu_2\nu_2,\mu_3\nu_3]} = & \left(\frac{1}{-M - \mathbb{I}\left[(\mu_1-\nu_1)i\omega_1 - (\mu_1+\nu_1)\frac{\Gamma_1}{2} + (\mu_2-\nu_2)i\omega_2 - (\mu_2+\nu_2)\frac{\Gamma_2}{2} + (\mu_3-\nu_3)i\omega_3 - (\mu_3+\nu_3)\frac{\Gamma_3}{2}\right]}\right) \\ \times \Big(&\mu_1(i\varepsilon_1 T_+)\mathbf{w}_{\mathrm{ss}[0\nu_1,\mu_2\nu_2,\mu_3\nu_3]} + \nu_1(-i\varepsilon_1 T_-)\mathbf{w}_{\mathrm{ss}[\mu_1 0,\mu_2\nu_2,\mu_3\nu_3]} + \mu_2(i\varepsilon_2 T_+)\mathbf{w}_{\mathrm{ss}[\mu_1\nu_1,0\nu_2,\mu_3\nu_3]} + \nu_2(-i\varepsilon_2 T_-)\mathbf{w}_{\mathrm{ss}[\mu_1\nu_1,\mu_2 0,\mu_3\nu_3]} \\ &+ \mu_3(i\varepsilon_3 T_+)\mathbf{w}_{\mathrm{ss}[\mu_1\nu_1,\mu_2\nu_2,0\nu_3]} + \nu_3(-i\varepsilon_3 T_-)\mathbf{w}_{\mathrm{ss}[\mu_1\nu_1,\mu_2\nu_2,\mu_3 0]}\Big)\end{aligned} \tag{A6}$$

down to the vector $\mathbf{w}_{\mathrm{ss}[00,00,00]} = \mathbf{v}^{\mathrm{ss}}$.

According to the quantum regression theorem the vector $\mathbf{y}$ defined as:

$$\mathbf{y}_{[11,\mu_2\nu_2,\mu_3\nu_3]}(t) = \begin{pmatrix} \langle n_1(0)(\varsigma_2^{\dagger\mu_2}\varsigma_2^{\nu_2})(t)(\varsigma_3^{\dagger\mu_3}\varsigma_3^{\nu_3})(0)\rangle \\ \langle n_1(0)(\varsigma_2^{\dagger\mu_2}\varsigma_2^{\nu_2}a)(t)(\varsigma_3^{\dagger\mu_3}\varsigma_3^{\nu_3})(0)\rangle \\ \langle n_1(0)(\varsigma_2^{\dagger\mu_2}\varsigma_2^{\nu_2}a^\dagger)(t)(\varsigma_3^{\dagger\mu_3}\varsigma_3^{\nu_3})(0)\rangle \\ \langle n_1(0)(\varsigma_2^{\dagger\mu_2}\varsigma_2^{\nu_2}a^\dagger a)(t)(\varsigma_3^{\dagger\mu_3}\varsigma_3^{\nu_3})(0)\rangle \end{pmatrix} \tag{A7}$$

satisfies the same equation of motion as the vector $\mathbf{w}_{[00,\mu_2\nu_2,00]}$, namely Eq. (2), with initial condition $\mathbf{y}_{[11,\mu_2\nu_2,\mu_3\nu_3]}(0) = \mathbf{w}_{\mathrm{ss}[11,\mu_2\nu_2,\mu_3\nu_3]}$. We can further define a vector:

$$\mathbf{z}_{[11,11,\mu_3\nu_3]}(t,t') = \begin{pmatrix} \langle n_1(0)n_2(t)(\varsigma_3^{\dagger\mu_3}\varsigma_3^{\nu_3})(t')\rangle \\ \langle n_1(0)n_2(t)(\varsigma_3^{\dagger\mu_3}\varsigma_3^{\nu_3}a)(t')\rangle \\ \langle n_1(0)n_2(t)(\varsigma_3^{\dagger\mu_3}\varsigma_3^{\nu_3}a^\dagger)(t')\rangle \\ \langle n_1(0)n_2(t)(\varsigma_3^{\dagger\mu_3}\varsigma_3^{\nu_3}a^\dagger a)(t')\rangle \end{pmatrix} \tag{A8}$$

which obeys the same equation of motion as $\mathbf{w}_{[00,00,\mu_3\nu_3]}$ [Eq. (2) with $t \to t'$] with initial conditions $\mathbf{z}_{[11,11,\mu_3\nu_3]}(t,0) = \mathbf{y}_{[11,11,\mu_3\nu_3]}(t)$. At last, the three photon spectrum is obtained, based on the definition of Eq. (3), as:

$$g^{(3)}_{\Gamma_1\Gamma_2\Gamma_3}(0,\omega_1;t,\omega_2;t',\omega_3) = \frac{\left[\mathbf{z}_{[11,11,11]}(t,t')\right]_1}{\left[\mathbf{w}_{\mathrm{ss}[11,00,00]}\right]_1\left[\mathbf{w}_{\mathrm{ss}[00,11,00]}\right]_1\left[\mathbf{w}_{\mathrm{ss}[00,00,11]}\right]_1}, \tag{A9}$$

where $[\cdots]_1$ denotes the first element of a vector. Likewise, the two photon spectrum is given by:

$$g^{(2)}_{\Gamma_1\Gamma_2}(0,\omega_1;t,\omega_2) = \frac{\left[\mathbf{y}_{[11,11,00]}(t)\right]_1}{\left[\mathbf{w}_{\mathrm{ss}[11,00,00]}\right]_1\left[\mathbf{w}_{\mathrm{ss}[00,11,00]}\right]_1}, \tag{A10}$$

and the one photon spectrum is given by $g^{(1)}_{\Gamma_1}(0,\omega_1) = \left[\mathbf{w}_{\mathrm{ss}[11,00,00]}\right]_1$

All the computations shown in the main text were performed recursively with Mathematica$^{\mathrm{TM}}$ using parameterized functions of solutions to the relevant differential equations. First all steady-state quantities were computed, followed by $\mathbf{y}_{[11,\mu_2\nu_2,\mu_3\nu_3]}(t)$ and $\mathbf{z}_{[11,11,\mu_3\nu_3]}(t,t')$. The coupling constants ϵ_i cancel out in the final normalized expressions for the two photon and three photon spectra.

[1] C. Cohen-Tannoudji and S. Reynaud, Phil. Trans. R. Soc. Lond. A **293**, 223 (1979).

[2] A. Aspect, G. Roger, S. Reynaud, J. Dalibard, and

C. Cohen-Tannoudji, Phys. Rev. Lett. **45**, 617 (1980).
[3] C. A. Schrama, G. Nienhuis, H. A. Dijkerman, C. Steijsiger, and H. G. M. Heideman, Phys. Rev. A **45**, 8045 (1992).
[4] M. Peiris, B. Petrak, K. Konthasinghe, Y. Yu, Z. C. Niu, and A. Muller, Phys. Rev. B **91**, 195125 (2015).
[5] A. González-Tudela, F. P. Laussy, C. Tejedor, M. J. Hartmann, and E. del Valle, New J. of Phys. **15**, 033036 (2013).
[6] V. N. Shatokhin and S. Y. Kilin, Phys. Rev. A **94**, 033835 (2016).
[7] P. Michler, A. Kiraz, C. Becher, W. Schoenfeld, P. Petroff, L. Zhang, E. Hu, and A. Imamoglu, Science **290**, 2282 (2000).
[8] R. H. Brown and R. Twiss, Nature **178**, 1046 (1956).
[9] J. Wiersig, C. Gies, F. Jahnke, M. Aßmann, T. Berstermann, M. Bayer, C. Kistner, S. Reitzenstein, C. Schneider, S. Höfling, A. Forchel, C. Kruse, J. Kalden, and D. Hommel, Nature **460**, 245 (2009).
[10] M. Aßmann, F. Veit, M. Bayer, M. van der Poel, and J. M. Hvam, Science **325**, 297 (2009).
[11] D. Elvira, X. Hachair, V. B. Verma, R. Braive, G. Beaudoin, I. Robert-Philip, I. Sagnes, B. Baek, S. W. Nam, E. A. Dauler, I. Abram, M. J. Stevens, and A. Beveratos, Phys. Rev. A **84**, 061802 (2011).
[12] M. J. Stevens, S. Glancy, S. W. Nam, and R. P. Mirin, Opt. Express **22**, 3244 (2014).
[13] A. Rundquist, M. Bajcsy, A. Majumdar, T. Sarmiento, K. Fischer, K. G. Lagoudakis, S. Buckley, A. Y. Piggott, and J. Vučković, Phys. Rev. A **90**, 023846 (2014).
[14] S. Bounouar, M. Strauß, A. Carmele, P. Schnauber, A. Thoma, M. Gschrey, J.-H. Schulze, A. Strittmatter, S. Rodt, A. Knorr, and S. Reitzenstein, Phys. Rev. Lett. **118**, 233601 (2017).
[15] E. Schlottmann, M. von Helversen, H. A. M. Leymann, T. Lettau, F. Krüger, M. Schmidt, C. Schneider, M. Kamp, S. Höfling, J. Beyer, J. Wiersig, and S. Reitzenstein, Phys. Rev. Applied **9**, 064030 (2018).
[16] E. del Valle, A. González-Tudela, F. P. Laussy, C. Tejedor, and M. J. Hartmann, Phys. Rev. Lett. **109**, 183601 (2012).
[17] J. C. López Carreño, E. del Valle, and F. P. Laussy, Laser Photonics Rev. **11**, 1700090 (2017).
[18] C. Sánchez Muñoz, E. del Valle, A. González Tudela, K. Müller, S. Lichtmannecker, M. Kaniber, C. Tejedor, J. J. Finley, and F. P. Laussy, Nat. Photonics **8**, 550 (2014).
[19] B. R. Mollow, Phys. Rev. **188**, 1969 (1969).
[20] F. Schuda, C. R. Stroud Jr, and M. Hercher, J. Phys. B: At. Mol. Phys. **7**, L198 (1974).
[21] G. Wrigge, I. Gerhardt, J. Hwang, G. Zumofen, and V. Sandoghdar, Nat. Phys. **4**, 60 (2008).
[22] A. Muller, E. B. Flagg, P. Bianucci, X. Y. Wang, D. G. Deppe, W. Ma, J. Zhang, G. J. Salamo, M. Xiao, and C. K. Shih, Phys. Rev. Lett. **99**, 187402 (2007).
[23] E. B. Flagg, A. Muller, J. W. Robertson, S. Founta, D. G. Deppe, M. Xiao, W. Ma, G. J. Salamo, and C. K. Shih, Nat. Phys. **5**, 203 (2009).
[24] S. M. Ulrich, S. Ates, S. Reitzenstein, A. Löffler, A. Forchel, and P. Michler, Phys. Rev. Lett. **106**, 247402 (2011).
[25] X. Xu, B. Sun, P. R. Berman, D. G. Steel, A. S. Bracker, D. Gammon, and L. J. Sham, Science **317**, 929 (2007).
[26] C. Roy and S. Hughes, Phys. Rev. Lett. **106**, 247403 (2011).
[27] O. Astafiev, A. M. Zagoskin, A. A. Abdumalikov Jr., Y. A. Pashkin, T. Yamamoto, K. Inomata, Y. Nakamura, and J. S. Tsai, Science **327**, 840 (2010).
[28] H. J. Kimble, Nature **453**, 1023 (2008).
[29] J. H. Eberly and K. Wódkiewicz, J. Opt. Soc. Am **67**, 1252 (1977).
[30] L. Knöll, G. Weber, and T. Schafer, J. Phys. B: At. Mol. Phys. **17**, 4861 (1984).
[31] R. Centeno Neelen, D. M. Boersma, M. P. van Exter, G. Nienhuis, and J. P. Woerdman, Opt. Commun. **100**, 289 (1993).
[32] K. Konthasinghe, J. Walker, M. Peiris, C. K. Shih, Y. Yu, M. F. Li, J. F. He, L. J. Wang, H. Q. Ni, Z. C. Niu, and A. Muller, Phys. Rev. B **85**, 235315 (2012).
[33] B. Petrak, M. Peiris, and A. Muller, Rev. Sci. Instrum. **86**, 023104 (2015).
[34] C. A. Schrama, G. Nienhuis, H. A. Dijkerman, C. Steijsiger, and H. G. M. Heideman, Phys. Rev. Lett. **67**, 2443 (1991).
[35] A. Ulhaq, S. Weiler, S. M. Ulrich, R. Roßbach, M. Jetter, and P. Michler, Nat. Photonics **6**, 238 (2012).
[36] J. Claudon, J. Bleuse, N. S. Malik, M. Bazin, P. Jaffrennou, N. Gregersen, C. Sauvan, P. Lalanne, and J.-M. Gérard, Nat. Photonics **4**, 174 (2010).
[37] M. Gschrey, A. Thoma, P. Schnauber, M. Seifried, R. Schmidt, B. Wohlfeil, L. Krüger, J.-H. Schulze, T. Heindel, S. Burger, *et al.*, Nat. Commun. **6**, 7662 (2015).
[38] L. Sapienza, M. Davanço, A. Badolato, and K. Srinivasan, Nat. Commun. **6**, 7833 (2015).
[39] C. Sánchez Muñoz, F. P. Laussy, E. del Valle, C. Tejedor, and A. González-Tudela, Optica **5**, 14 (2018).